Ribosome-binding protein 1, RRBP1, maintains peroxisomal biogenesis

Kaneez Fatima[1], Helena Vihinen[2], Bala Ani Akpinar[1], Tamara Somborac[1], Eija Jokitalo[2], Pekka Katajisto[3], Svetlana Konovalova[1]*

[1] Institute of Biotechnology, Helsinki Institute of Life Science (HiLIFE), University of Helsinki, Helsinki, Finland

[2] Electron Microscopy Unit, Institute of Biotechnology, Helsinki Institute of Life Science (HiLIFE), University of Helsinki, Helsinki, Finland

[3] Faculty of Biological and Environmental Sciences, University of Helsinki, Helsinki, Finland

*Corresponding author

Keywords: peroxisome, RRBP1, CRISPR/Cas9, contact sites

ABSTRACT

Peroxisomes are single membrane-bound organelles essential for human health, yet the mechanism of peroxisomal biogenesis remains poorly described. Here using a systematic double screening approach, we identified ribosome-binding protein 1, RRBP1, as a novel peroxisomal biogenesis factor in human cells. We showed that the number of peroxisomes and the levels of peroxisomal proteins are reduced by RRBP1 KO in HEK293T cells. In addition, the processing of peroxisomal matrix proteins, such as ACOX1 and thiolase was affected in RRBP1 KO HEK293T cells. Using electron microscopy, we showed that RRBP1, an ER membrane protein, is involved in the maintaining of the long-distance contact sites between ER and peroxisomal membranes, suggesting that the role of RRBP1 in peroxisomal biogenesis is mediated through inter-organellar contact sites. Altogether our results showed that RRBP1 promotes peroxisomal biogenesis in human cells highlighting the power of systematic approaches in discovering novel factors of organellar biogenesis.

INTRODUCTION

Peroxisomes are single membrane-bounded organelles, essential for their role in lipid breakdown and specifically in the β-oxidation of long-chain fatty acids. The *de novo* peroxisomal biogenesis starts with the assembly of peroxisomal membrane receptors PEX3 and PEX16, which together ensure the import of peroxisomal membrane proteins recognized by cytosolic chaperone PEX19. Once the import machinery is assembled on the membranes, peroxisomes are ready to import matrix proteins translated on free ribosomes and imported post-translationally directly from the cytosol (Goldman and Blobel, 1978; Hasan et al., 2013; Rachubinski et al., 1984). Most of the peroxisomal matrix proteins contain targeting sequences, PTS1 or PTS2, that are recognized by cytosolic peroxins, PEX5 or PEX7 respectively (Walter and Erdmann, 2019; Okumoto et al., 2018). The translocation of the substrate proteins into the peroxisomal matrix is mediated by factors localized on the peroxisomal membrane such as PEX14, PEX13, and PEX26 (Schliebs et al., 1999; Albertini et al., 1997; Distel et al., 1996; Matsumoto et al., 2003). Although studies in yeast (Akşit and van der Klei, 2018; Erdmann et al., 1989) and mammalian cells (Fang et al., 2004; Fujiki et al., 2014) have identified core components required for peroxisomal matrix import, many aspects of peroxisomal protein biogenesis remain unclear.

No systematic approach has been previously applied to reveal peroxisomal biogenesis factors in human cells. To systematically identify factors involved in biogenesis of peroxisomes we first utilized APEX2-proximity labeling followed by mass spectrometry as a powerful tool to study protein-protein interactions. Using this approach, we revealed factors that specifically interact with peroxisomal matrix cargo. Secondly, we tested these factors by CRISPR-Cas9 KO microscopy screening. Using this double screening approach we identified ribosome-binding protein 1, RRBP1, as a novel peroxisomal biogenesis factor. Using knockout and knockdown models we observed the loss of peroxisomes in cells lacking or depleted for RRBP1. Using confocal microscopy, we showed less overlap between ER and peroxisomes upon RRBP1 KO, suggesting that RRBP1 is

involved in the formation of membrane contact sites between ER and peroxisomes. High-resolution electron microscopy imaging showed that RRBP1 KO indeed affects peroxisome-ER contacts, specifically it reduces long-distance contact sites between peroxisomes and ER. Thus, our study showed that RRBP1 is required for peroxisomal maintenance in human cells.

RESULTS

Systematic identification of peroxisomal biogenesis factors using a double screening approach

To systematically identify factors required for the protein import into the peroxisomal matrix we first used a proximity-labeling approach followed by mass spectrometry (Fig. 1A). Ascorbate peroxidase (APEX2) was fused to the ePTS1, peroxisomal targeting sequence recognized by PEX5 and directing the construct to the peroxisomal matrix. The GFP-APEX2-ePTS1 construct was stably expressed in HEK293T control cells or cells lacking peroxisomes (PEX3 KO or PEX19 KO cells, Fig. 1B). The GFP-APEX2-ePTS1 construct is recognized by peroxisomal protein import factors and in control cells delivered to the peroxisomal matrix, however, in PEX3 KO or PEX19 KO cells the construct stayed in the cytosol due to the absence of peroxisomes (Fig 1C). Thus, the factors required for the delivery of ePTS1-containing proteins to peroxisomes are expected to stack near the GFP-APEX2-ePTS1 construct in PEX3 KO or PEX19 KO cells. Therefore, the proteins that were specifically found in close proximity to the ePTS1 construct in PEX3 KO or PEX19 KO cells were selected as potential peroxisomal biogenesis factors. To exclude non-specifically labeled proteins we used parental cells without expressing construct and cells stably expressing non-targeted GFP-APEX2.

Biotinylated proteins were extracted using streptavidin beads and analyzed by mass spectrometry. Proteins identified in two replicates for each PEX3 KO and PEX19 KO cells were considered as significant hits. To identify highly specific interactors of GFP-APEX2-ePTS1 in cells lacking

peroxisomes we excluded any protein identified in background samples (Supplementary Table 1). Next, we excluded essential proteins (Supplementary Table 2), and based on the pathway analysis of the candidates we selected 44 proteins potentially involved in peroxisomal biogenesis (Fig. 1D,E, Supplementary Table 3).

To analyze the involvement of these candidates in peroxisomal biogenesis we performed a secondary screen using CRISPR/Cas9 and microscopy (Fig. 2A). We generated two gRNAs targeting each of the 44 candidates identified by proximity labeling. HEK293T cells stably expressing GFP-APEX2-ePTS1 were used as a reporter cell line. The cells were co-transfected with the Cas9 plasmid and individual gRNAs. Live-cell fluorescent microscopy was performed to examine the localization of GFP in the transfected cells, using the relocalization of GFP signal from the peroxisomes to the cytosol to identify gRNAs that target genes potentially important for peroxisomal biogenesis. The phenotype of the cells was analyzed using live-cell microscopy and scored based on the localization of the GFP signal from 0 to 3, where 0 corresponded to GFP localized in peroxisome puncta and 3 for strong mislocalization of GFP to the cytosol. Two rounds of transfections were performed for each gRNA, each time the cells were analyzed three times at 7, 10, and 14 post-transfection days. As a positive control, we used gRNAs targeting known essential peroxisomal assembly factors, such as PEX5 and PEX19 (Fig. 2B, C). Using this double-screening approach we identified potential factors required for peroxisomal biogenesis (Fig. 2B). The top three candidates included tyrosine-protein phosphatase non-receptor type 1 (PTN1), glycerol-3-phosphate phosphatase (PGP) and ribosome-binding protein 1 (RRBP1) (Fig. 2B).

RRBP1 is required for peroxisomal maintenance in human cells

Our double-screening approach identified RRBP1 as a potential peroxisomal biogenesis factor. To investigate the involvement of RRBP1 in the maintenance of peroxisomes we generated RRBP1

KO HEK293T clonal cell line expressing the GFP-APEX2-ePTS1 construct by CRISPR/Cas9-based editing. To achieve a complete knockout of the RRBP1 gene we used a sgRNA targeting an exon common to all isoforms of RRBP1, exon 2. Using immunoblotting we confirmed the complete depletion of the RRBP1 protein in the generated RRBP1 KO cell line (Fig. 3A). We analyzed RRBP1 KO HEK293T cells expressing GFP-APEX2-ePTS1 and its parental cell line as a control. In addition, as a positive control we used cells lacking essential peroxisomal biogenesis factors, PEX3 or PEX19, generated in our previous study (Somborac et al., 2023). We observed that the steady-state protein levels of peroxisomal matrix protein, catalase, as well as the peroxisomal membrane proteins, PEX3 and PEX19 were decreased in RRBP1 KO cells compared to the parental cell line (Fig. 3A, B). Interestingly, the protein level of PEX5, an essential peroxisomal matrix protein factor, was induced upon RRBP1 KO (Fig. 3A, B).

Next, we analyzed the peroxisomal function in RRBP1 KO cells by assessing peroxisomal matrix protein import. Although most of the peroxisomal proteins are translated in the cytosol in their mature form, some peroxisomal proteins undergo processing upon import to peroxisomes. Once imported to the peroxisomal matrix, the 72 kDa cytosolic unprocessed acyl-CoA oxidase 1, ACOX1, a PTS1-targeted peroxisomal matrix protein is cleaved into its 50 kDa and 22 kDa mature forms (Kurochkin et al., 2007). Similarly, 44 kDa unprocessed 3-ketoacyl-CoA thiolase, ACAA1, a PTS2-targeted peroxisomal matrix protein, upon impot to peroxisomes is processed to 42 kDa (Miura et al., 1984). Using immunoblotting we showed that the processing of ACOX1 and ACAA1 was abolished in cells lacking peroxisomes, PEX3 or PEX19 KO cells (Fig. 3A, C), confirming that this assay can be efficiently used to analyze peroxisomal function as shown previously (Klouwer et al., 2021; Kurochkin et al., 2007). Using immunoblotting analysis, we observed a significant decrease in the processing of both tested peroxisomal matrix proteins, ACOX1 and ACAA1 upon RRBP1 KO.

Notably, PEX3 KO or PEX19 KO cells have significantly lower RRBP1 protein levels compared to their parental cells, indicating that RRBP1 protein is responsive to the absence of peroxisomes. The protein levels of calnexin and VAPB, endoplasmic reticulum proteins involved in ER stress response, were slightly decreased in RRBP1 KO cells compared to the parental cells (Fig. 3D), indicating that RRBP1 KO affects ER, but does not induce ER stress. We observed no effect of RRBP1 KO on the steady state level of mitochondrial protein, TOM20 (Fig. 3E), suggesting that mitochondrial mass is not affected in cells lacking RRBP1.

Altogether these results show that RRBP1 is an important factor involved in the maintenance of peroxisomes in human cells.

RRBP1 KO causes a decreased number of peroxisomes in human cells

Next, we investigated whether the peroxisomal number is affected by RRBP1 KO. We used RRBP1 KO HEK293T cells stably expressing GFP-APEX2-ePTS1 and its parental cell line as a negative control. Live-cell fluorescent microscopy analysis showed that RRBP1 KO cells have less GFP-positive dots representing peroxisomes compared to the parental cells (Fig. 4A). In addition, GFP-APEX2-ePTS1 was partially localized to cytosol in cells lacking RRBP1, while in parental HEK293T cells the construct was correctly localized to peroxisomes, confirming our result from CRISPR screen (Fig. 2C). These data show that the import of peroxisomal matrix proteins is affected by RRBP1 KO.

To study if RRBP1 KO also affects peroxisome numbers, we performed high-resolution immunofluorescence confocal microscopy of RRBP1 KO cells using PEX14 as a membrane marker and catalase as a matrix marker of peroxisomal structures. As a positive control we used cells lacking peroxisomes, PEX3 KO or PEX19 KO HEK293T cells. The number of PEX14- or catalase-positive structures per cell were reduced in RRBP1 KO cells compared to the parental cells (Fig. 4

B-D), confirming that RRBP1 indeed is required for peroxisomal maintenance. The volume of the cells was not affected upon RRBP1 KO, and thus the volume of the cells does not contribute to the reduced number of peroxisomal structures per cell in RRBP1 KO cells (Fig. 4E).

Notably, the number of PEX14-positive structures dropped by around 30%, while the number of catalase-positive structures dropped by 45% (Fig. 4C, D). It is known that during biogenesis early peroxisomes (pre-peroxisomes) contain only membrane proteins and later during the maturation process the matrix proteins are imported (Dimitrov et al., 2013; Titorenko and Rachubinski, 2008). Thus, catalase, labels only mature peroxisomes, while PEX14 presents in both pre-peroxisomes and mature peroxisomes. Our data indicate that the relative number of pre-peroxisomes out of the total peroxisome pool calculated as a difference between PEX14-positive dots and catalase-positive dots is higher in RRBP1 KO (50%) compared to the parental cells (35%) (Fig. 4F). These data suggest that RRBP1 KO also affects the maturation of the peroxisomes.

RRBP1 silencing causes peroxisomal deficiency in human cells

To validate our findings on RRBP1 KO cells we knocked down RRBP1 using esiRNA in HEK293T cells stably expressing GFP-APEX2-ePTS1. GFP esiRNA was used as a negative control while esiRNA targeting peroxisomal import factor essential for the assembly of functional peroxisomes, PEX5, was used as a positive control. Protein levels of ACAA1 and catalase analyzed by immunoblotting were reduced upon RRBP1 silencing (Fig. 5A, B, D). The processing of ACOX1 was significantly decreased in cells transfected with RRBP1 esiRNA (Fig. 5C). Using live-cell fluorescent microscopy imaging we showed mislocalization of GFP-APEX2-ePTS1 construct to the cytosol in cells transfected with RRBP1 esiRNA (Fig. 5E).

Thus, we showed that RRBP1 silencing similarly to RRBP1 KO causes peroxisomal deficiency, indicating that RRBP1 is specifically involved in the maintenance of peroxisomes in human cells.

The decreased number of peroxisomes in RRBP1 KO cells is independent of pexophagy

We showed that the steady state number of peroxisomes is decreased upon RRBP1 KO. Peroxisomal homeostasis is regulated by the interplay between peroxisomal biogenesis and selective autophagy of peroxisomes, pexophagy (Demers et al., 2023; Germain and Kim, 2020; Sakai et al., 2006). Therefore, the decreased peroxisomal number upon RRBP1 KO could be the result of affected peroxisomal biogenesis where less peroxisomes were formed or induced pexophagy leading to the loss of peroxisomes. To distinguish these two possibilities, we tested whether pexophagy is induced in RRBP1 KO cells. We showed that the steady-state levels of autophagy markers, such as LC3B and ATG5 were reduced in RRBP1 KO cells compared to the parental cell line (Fig. 6A, B). To test if blocking pexophagy could rescue the levels of peroxisomal makers in RRBP1 KO cells we treated cells with chloroquine (100 µM, 3 h), which inhibits fusion of autophagosomes with lysosomes. The inhibition of autophagy upon chloroquine treatment was confirmed by induction of LC3B-II, indicating the accumulation of autophagosomes (Fig. 6A, B).

We did not observe rescue of PEX3 or PMP70 protein levels upon chloroquine treatment in cells lacking RRBP1 (Fig. 6A, B). These results suggest that pexophagy is not induced in RRBP1 KO cells therefore it does not contribute to the decreased number of peroxisomes in cells lacking RRBP1 is likely due to its role in peroxisomal biogenesis.

RRBP1 does not localize to peroxisomes

Our data showed that RRBP1 maintains peroxisomal biogenesis. Previously, RRBP1 was described as an ER transmembrane protein (Shibata et al., 2010; Ogawa-Goto et al., 2007; Savitz and Meyer, 1990), suggesting that the role of RRBP1 in peroxisomal biogenesis is mediated through the ER. To analyze whether in addition to ER, RRBP1 is localized to peroxisomes we performed colocalization

analysis using confocal microscopy and corresponding antibodies labeling peroxisomes, ER, or mitochondria (Fig. 7A). RRBP1 mainly localized to ER, showed some localization to mitochondria, while we observe very week colocalization of RRBP1 with peroxisomes (Fig. 7A,B). Thus, our data suggest that RRBP1 is not a part of peroxisomal import machinery, instead its role in peroxisomal biogenesis is mediated by ER.

RRBP1 KO affects peroxisome-ER contact sites

Recent studies suggest that RRBP1 can act as a tether in contact sites between ER and mitochondrial membranes ensuring metabolic communication between two organelles (Hung et al., 2017; Anastasia et al., 2021). We hypothesized that RRBP1 could be involved in peroxisomal biogenesis via ER contact sites. To test whether RRBP1 has a role in peroxisome-ER contact sites we used confocal microscopy to analyze the overlap between the ER marker calnexin and the peroxisomal marker PMP70 in RRBP1 KO and parental cells. We observed less colocalization between ER and peroxisomes in RRBP1 KO cells compared to the parental HEK293T cell line (Fig. 8A,B). Notably, in agreement with the previous study (Hung et al., 2017), the colocalization of ER with mitochondria was not affected in RRBP1 KO cells (Fig. 8A,B).

To study the specific role of RRBP1 in maintaining peroxisome-ER contacts we used electron microscopy. We took advantage of APEX2, a well-characterized powerful tool for labeling intracellular structures in electron microscopy studies (Martell et al., 2017; Rae et al., 2021; Sengupta et al., 2019; Lam et al., 2014). Using DAB staining we labeled peroxisomes in RRBP1 KO HEK293T cells stably expressing GFP-APEX2-ePTS1 and its parental cell line (Fig. 8C). For the analysis of peroxisome-ER contact sites three independent experiments were performed. In each experiment for each cell line 13-18 cells having peroxisomal profiles were selected using systematic random sampling. All the peroxisomes in the selected cells were imaged (n = 437 for the parental cell line, n = 403 for the RRBP1 KO cell line) and the peroxisomal-ER distances were analyzed

using Microscopy Image Browser (MIB, (Belevich et al., 2016)). We assessed the occurrence of contact sites between peroxisomes and ER at two distance categories, short distances (50-60 nm) and long distances (90-105 nm). We observed less long-distance contact sites between peroxisomes and ER in RRBP1 KO cells compared to the parental cells, while peroxisome-ER short-distance contacts were not affected by RRBP1 KO (Fig. 8D).

In addition, by using electron microscopy images we analyzed peroxisomal morphology upon RRBP1 KO. Although the size and shape of peroxisomes varied, there were no changes in peroxisomal size or shape upon RRBP1 KO (Fig. 8E,F).

Altogether, the data suggest that RRBP1 can be involved in the formation of contact sites between ER and peroxisomes and potentially promotes peroxisomal biogenesis through ER-peroxisome contact sites.

DISCUSSION

We have here identified and characterized a novel peroxisomal biogenesis factor, RRBP1. RRBP1 also known as p180/ribosome receptor, is a transmembrane ER protein with a poorly understood function. RRBP1 was originally identified as a ribosome receptor for the ER (Savitz and Meyer, 1990); it was also proposed to interact with microtubules (Ogawa-Goto et al., 2007) and microtubule-dependent motor protein, kinesin (Diefenbach et al., 2004). Recent studies suggest that RRBP1 plays a role in tethering ER with mitochondria (Anastasia et al., 2021; Cardoen et al., 2024; Hung et al., 2017) and regulates mitophagy (Killackey et al., 2023). However, RRBP1 has never been linked to peroxisomal function before. Using a powerful systematic approach, we were able to reveal RRBP1 as a factor involved in peroxisomal biogenesis.

We showed that the cells lacking RRBP1 lose peroxisomes. However, in contrast to the cells lacking essential components of peroxisomal biogenesis machinery, such as PEX3 and PEX19, we did not see the complete absence of peroxisomes in RRBP1 KO cells, indicating that although RRBP1 plays a role in peroxisomal biogenesis it is not an essential factor.

Interestingly, in RRBP1 KO cells as well as in the cells completely lacking peroxisomes, PEX3 KO or PEX19 KO cells, we observed induction of PEX5 protein level, a cytosolic peroxin essential for protein delivery into the peroxisomal matrix. These data indicate that the loss of peroxisomes in RRBP1 KO cells mediates cellular response to compensate for peroxisomal deficiency by inducing peroxisomal biogenesis factors.

We showed that the number of both peroxisomal structures containing membrane marker PEX14 and matrix marker catalase decreased in RRBP1 KO cells. However, we noted that the number of matrix-labeled structures, labeling mature peroxisomes, is more reduced. Quantification analysis showed that RRBP1 KO cells have a lower percentage of mature peroxisomes compared to the parental cells. This phenomenon suggests that RRBP1 is involved in the maturation of peroxisomes.

To test the possibility that the loss of peroxisomes in RRBP1 KO cells resulted from enhanced removal of peroxisomes we tested whether the decreased levels of peroxisomal proteins in RRBP1 KO cells can be rescued by blocking pexophagy. We did not observe the rescue of peroxisomal proteins in RRBP1 KO after pexophagy inhibition. Notably, the steady-state protein levels of LC3B were dramatically reduced in RRBP1 KO cells, suggesting. Altogether, these results indicate that pexophagy does not play a role in the loss of peroxisomes in RRBP1 KO cells. In fact, pexophagy rate is reduced in RRBP1 KO cells, probably due to the fewer peroxisomes present in these cells.

It is interesting to show that peroxisomal biogenesis in human cells requires RRBP1, an ER membrane protein. Using confocal microscopy, we showed that RRBP1 is not localized to peroxisomes, thus making it unlikely that RRBP1 is directly involved in peroxisomal protein import. The classical model of peroxisomal biogenesis suggests that peroxisomal membranes originate from ER in the form of budding pre-peroxisomal vesicles (Lam et al., 2010). However, our APEX2-based proximity labeling suggests that RRBP1 interacts with cargo proteins containing PTS1 peroxisomal targeting signal, proposing that RRBP1 has a role in the import of peroxisomal matrix proteins. Importantly, in contrast to peroxisomal membrane proteins, peroxisomal matrix proteins are not detected in ER (Geuze et al., 2003; Van Der Zand et al., 2010). Therefore, our data suggests that RRBP1 is not directly involved in the delivery of peroxisomal matrix proteins, instead, it can facilitate the recruitment to the peroxisomal membranes of other factors required for the protein import into the peroxisomal matrix.

How is ER protein can be involved in peroxisomal biogenesis? Recent studies suggest that peroxisomes closely interact with ER via connections called membrane contact sites, playing an important role in the peroxisomal dynamics, biogenesis, and metabolic signaling (Costello et al., 2017; Hua et al., 2017; Guillén-Samander et al., 2021; Baldwin et al., 2021). Our confocal microscopy analysis showed less colocalization between ER and peroxisomes in RRBP1 KO cells compared to the parental cells, suggesting RRBP1 role in the formation of peroxisome-ER contacts.

RRBP1 is a long transmembrane protein, and its full length contains 1410 amino acids, its C-terminal cytosolic domain constitutes 98% of the protein. Therefore, contacts formed by RRBP1 are more likely to be of long distance. Consistent with this possibility, using electron microscopy imaging we showed that RRBP1 KO affects specifically long-distance peroxisome-ER contact sites.

These data raise the intriguing possibility that RRBP1 could be involved in peroxisomal biogenesis by interrupting peroxisome-ER contact sites. Notably, in cells lacking peroxisomes PEX3 KO or PEX19 KO cells, the RRBP1 protein level was reduced, suggesting that RRBP1 is responsive to the absence of peroxisomes. As RRBP1 is involved in the formation of peroxisome-ER contact sites, the reduction of RRBP1 protein in PEX3 KO or PEX19 KO cells can be explained by the loss of peroxisomes.

So far, the only well-characterized tethering complex mediating membrane contact sites between ER and peroxisomes is the VAPB-ACBD5 (Kors et al., 2022; Hua et al., 2017; Costello et al., 2017). In addition, a recent study identified vacuolar protein sorting 13 homolog D, VPS13D, as a factor promoting peroxisomal biogenesis. VPS13D was shown to bridge ER to both peroxisomes and mitochondria via Miro protein ensuring lipid transport between organelles (Guillén-Samander et al., 2021; Baldwin et al., 2021), highlighting the importance of peroxisome-ER contact sites in peroxisomal maintenance.

RRBP1 was previously shown to be involved in contact between ER and mitochondria (Anastasia et al., 2021; Cardoen et al., 2024; Hung et al., 2017). Thus, the fraction of mitochondria associated with wrapped by curved sheets of rough ER was enriched in RRBP1 protein compared to the ER control fraction. Silencing of RRBP1 expression in mouse liver caused remodeling of contacts between mitochondria and wrapped by curved sheets of rough ER, ultimately affecting liver lipid homeostasis (Anastasia et al., 2021). Notably, the peroxisomal membrane protein, PMP70, was co-fractionated with RRBP1 (Anastasia et al., 2021), suggesting the interaction of RRBP1 with peroxisomal membranes. Such interaction potentially facilitates inter-organellar metabolic

trafficking ensuring peroxisomal biogenesis. In addition, RRBP1 can act as the ribosome receptor that regulates local translation in axons (Koppers et al., 2022). Therefore, contacts between peroxisomes and ER formed by RRBP1 could mediate the local translation of peroxisomal proteins thus promoting peroxisomal biogenesis.

Interestingly, RRBP1 appears to be a metazoan-specific protein, its homologs are not found in yeast. Therefore, despite the conservativity of general protein targeting mechanisms in eukaryotic cells, the role of RRBP1 in peroxisomal biogenesis can represent a specific pathway of peroxisomal maintenance in higher eukaryotes.

In conclusion, the identification and characterization of RRBP1 as a peroxisomal biogenesis factor advances our understanding of organelle biogenesis, a complex process involving multiple steps and diverse intracellular cooperation.

MATERIALS AND METHODS

Cell culture

HEK293T cells (ATCC, CRL-11268) were cultured (37°C, 5% CO2) in DMEM (Pan-Biotech, P04-03600) supplemented with 10% fetal bovine serum (GIBCO, 10270106), l-glutamine (GIBCO, 25030081) and penicillin/streptomycin (GIBCO, 15140122). TransIT-X2 (MirusBio, MIR 6000) or TransIT2020 (Mirus, MIR 5400) were used for cell transfection according to manufacturer's instruction.

Generation of knockout cell lines

PEX3 KO and PEX19 KO HEK293T cells were generated in our previous study (Somborac et al., 2023) using CRISPR/Cas9 genome editing. Cells were co-transfected with two gRNAs and pSpCas9n(BB)-2A-Puro (PX462) V2.0 (Addgene, 62987 (Ran et al., 2013)). PEX3 gRNAs were ACGTGCTTGAAAGGGGGCAT and CACCTCCAAGGACCGTGCCC. PEX19 gRNA were GGGCCCCAGAAGAGATCGCC and GGGGCCGTGGTGGTAGAAGG. After 24 h the cells were selected with puromycin and expanded. T7 assay was used to confirm genome editing. Single cell clones were obtained and validated using immunoblotting analysis.

To generate RRBP1 KO HEK293T cells expressing EGFP-FLAG-APEX2-ePTS1 single gRNA transcriptional cassette prepared by PCR and pCAS9-mCherry empty (Addgene, 80975 (Schmid-Burgk et al., 2016)) were co-transfected into HEK293T cells expressing EGFP-FLAG-APEX2-ePTS1. After 24 h of transfection mCherry-positive cells were sorted by FACS onto 96-well plate containing DMEM media supplemented with 15% fetal bovine serum (GIBCO, 10270106), l-glutamine (GIBCO, 25030081) and penicillin/streptomycin (GIBCO, 15140122) and single cell clones generated. The RRBP1 KO cells were validated using immunoblotting analysis. Exon 1 in

RRBP1 is non-coding, therefore we used gRNA targeting the first coding exon common to all isoforms of RRBP1, exon 2. The sequence of sgRNA was CGAAGGAGGACAGTCACATT.

Plasmid construction

To generate GFP-APEX2-ePTS1 (pLL3.7-GFP-FLAG-APEX2-ePTS1) we used PCR overlap extension. FLAG-APEX2 fragment was amplified form pcDNA3 APEX2-NES (Addgene, 49386 (Lam et al., 2015)), ePTS1 was generated using corresponding primers. The resulting fused construct was inserted into pLL3.7 vector (11795 (Rubinson et al., 2003)) using EcoRI and NheI restriction sites. To generate GFP-APEX2 (pLL3.7-GFP-FLAG-APEX2) GFP-FLAG-APEX2 fragment was amplified from pLL3.7-GFP-FLAG-APEX2-ePTS1 plasmid and ligated into pLL3.7 vector. All plasmids were confirmed by Sanger sequencing. Primers used for the cloning are in Supplementary Table 4.

Stable cell line generation

HEK293T stably expressing GFP-APEX2-ePTS1 or GFP-APEX2 were generated by using standard lentiviral cell line generation protocol. Briefly, WT, PEX3 KO or PEX19 KO cells were co-transfected with pMD2.G (Addgene, 12259), psPAX2 (Addgene,12260) and pLL3.7-GFP-FLAG-APEX2-ePTS1 or pLL3.7-GFP-FLAG-APEX2 using TransIT-2020 (MirusBio, MIR 5400) following manufacturer's instructions. pMD2.G was a gift from Didier Trono (Addgene plasmid # 12259 ; http://n2t.net/addgene:12259 ; RRID:Addgene_12259). psPAX2 was a gift from Didier Trono (Addgene plasmid # 12260 ; http://n2t.net/addgene:12260 ; RRID:Addgene_12260). Single cell clones were obtained by FACS. The expression of the constructs was confirmed by immunoblotting.

APEX2-proximity labeling

APEX2-proximity labeling was performed using previously described protocol (Hung et al., 2016) with few modifications. HEK293T cells were grown on T75 flasks. The media was changes and 500 µM biotin-phenol was added to the cell culture media for 30 min (37°C, 5% CO2). Proximity labeling was induced by adding 10 mM of H_2O_2 (Fisher Scientific, BP2633-500). The reaction was stopped after 1 min, by removing the media and washing the cells with quencher solution (10 mM sodium ascorbate, 5 mM Trolox and 10 mM sodium azide solution in PBS). Cells were collected in 15 mL quencher solution and pelleted at 3 000 g at 4 °C for 10 min. Cell pellets were flash frozen in liquid nitrogen. When processing all cell lines was complete, pellets were lysed in RIPA lysis buffer supplemented with protease inhibitor cocktail (Thermo Scientific, 10320015), 1 mM PMSF, 5 mM Trolox, 10 mM sodium azide and 10 mM sodium ascorbate. Cell lysates were incubated on ice for about 2 min and then centrifuged at 15 000 g at 4 °C for 10 min. Streptavidin magnetic beads (Thermo Scientific, 88816) were washed twice with RIPA lysis buffer supplemented with protease inhibitor cocktail (Thermo Scientific, 10320015), 1 mM PMSF, 5 mM Trolox, 10 mM sodium azide and 10 mM sodium ascorbate. Then, clarified cell lysates were added to the beads and incubated overnight with rotation at 4 °C. Biotinylated proteins were eluted by boiling the beads in elution buffer (3× protein loading buffer supplemented with 2 mM biotin and 20 mM DTT) for 10 min. Tubes were briefly centrifuged and using a magnetic rack, samples were collected, flash frozen in liquid nitrogen and stored at -80 °C.

Frozen eluates were thawed on ice and run on 10% separating gel at 200 V for 9 min. Samples were cut from the gel, stained with Coomassie, and washed twice with H_2O. Then individual lanes were cut out and stored at -20 °C in separate microfuge tubes. Scalpels used to cut the gel were single use, and the samples were loaded with one empty well between.

Mass spectrometry analysis of proteins

Protein bands were cut out of the SDS-PAGE gel and “in-gel” digested. Cystein bonds were reduced with 0.045M dithiothreitol (Sigma-Aldrich, D0632) for 20 min at 37 °C and alkylated with 0.1 M iodoacetamide (Fluka, Sigma-Aldrich, 57670) at room temperature in the dark for 30 min. Proteins were digested with 0.75 µg trypsin (Sequencing Grade Modified Trypsin, V5111, Promega) overnight at 37 °C. After digestion, peptides were purified with C-18 Micro SpinColumns (The Nest Group Inc. USA) according to manufacturer’s instructions. The dried peptides were reconstituted in 30 µl 0.1% trifluoroacetic acid (TFA) and 1% acetonitrile (ACN) in LC-MS grade water. The mass spectrometry analysis was performed on an Orbitrap Elite and Q Exactive ESI-quadrupole-orbitrap mass spectrometer coupled to an EASY-nLC 1000 nanoflow LC (Thermo Fisher Scientific), using the Xcalibur version 3.1.66.10 (Thermo Scientific) as described in (Liu et al., 2018). Acquired spectral data files were searched against the human component of UniProtKB/SwissProt database using SEQUEST search engine in the Proteome Discoverer 1.4 (Thermo Scientific). The following parameters were applied: only fully tryptic peptides were allowed with maximum of two missed cleavages, precursor mass tolerance and fragment mass tolerance were set to ±15 ppm and 0.05 Da, respectively. Carbamidomethylation of cysteine was defined as static modification and oxidation of methionine was set as variable modification. The mass spectrometry data were filtered and presented as peptide spectrum matches.

esiRNA gene silencing

HEK293T cells expressing EGFP-FLAG-APEX2-ePTS1 were plated in 6-well plate 24 h before transfection. The cells were transfected with esiRNA targeting GFP (Merck, EHUEGFP), RRBP1 (Merck, EHU073471), or PEX5 (Merck, EHU090061) using TransIT-X2 (MirusBio, MIR 6000). After 72 h the cells were collected for immunoblotting analysis.

CRISPR/Cas9 microscopy screen

To perform CRISPR/Cas9 microscopy screen for each 44 selected candidates and two positive controls (PEX5 and PEX19) two gRNAs were designed, except for CSK21, for which only one target sequence was found with sufficient specificity. gRNAs with U6 overhang at 5' and terminator overhang at 3' were purchased as oligos (Supplementary Table 5). U6 was cloned from PX335-dCas9-VP192-PGKpuro using PCR. Obtained U6 was 5'-tailed and amplified using PCR. 3'-tailed terminator was generated using PCR. gRNA transcriptional cassette was generated by PCR using 5'-tailed U6, 3'-tailed terminator, and U6 overhang-gRNA-terminator overhang as described and utilized in (Balboa et al., 2015; Konovalova et al., 2023, 2018). The sequences of used oligos are in Supplementary Table 4.

HEK293T cells expressing EGFP-FLAG-APEX2-ePTS1 were plated in 24-well plates 24 h before the transfection. The cells were co-transfected with a single gRNA and pCAS9-mCherry empty (Addgene, 80975 (Schmid-Burgk et al., 2016)) using TransIT-2020 (Mirus, MIR 5400). The cells were passaged when needed. The cells were analyzed by live-cell fluorescent microscopy at 7, 10 and 14 post-transfection days using EVOS FLoid Imaging System (Thermo Fisher Scientific). The localization of GFP signal was scored from 0 to 3, where 0 corresponded to GFP localized strictly in puncta, 1 – some GFP signal mislocalized in cytosol, 2 – average level of GFP mislocalization to cytosol, and 3 is for strong mislocalization of GFP to cytosol.

Live-cell fluorescent microscopy

Live microscopy imaging was performed on cells in 6-weel or 24-well plates using EVOS FLoid Imaging System (Thermo Fisher Scientific) equipped with 20x objective or Eclipse TS100 (Nikon) equipped with 40× objective.

Western blotting

HEK293T cells were lysed in RIPA buffer (Cell Signaling, 9806S) supplemented with protease inhibitor cocktail (Thermo Scientific, 78429). Following 15 min incubation on ice, the samples were centrifuged at 14 000 g for 10 minutes at +4°C. Protein concentration was measured by bicinchoninic acid (BCA) assay (Thermo Fisher, 23228). Protein lysates were supplemented with a laemmli sample buffer (60 mM Tris-Cl pH 6.8, 2% SDS, 10% glycerol, 5% β-mercaptoethanol, 0.01% bromophenol blue), boiled for 5 min at 95° and resolved on 10 % or 7.5 % Mini-PROTEAN TGX Precast Gels (Bio-Rad, 4561033, 4561036, 4561023, 4561026). The SDS-PAGE was performed at 100 V for 5 minutes and then 120 V for 1 hour 15 minutes using SDS running buffer (30 g Tris, 144 g glycine, 10 g SDS to 1 L distilled water). Then the proteins were transferred to a 0.2-μM PVDF membrane (Bio-Rad, 1704150) by Trans-Blot Turbo Transfer System (Bio-Rad) using pre-installed settings (2.5 A for 7 min) for transferring proteins of mix molecular weight. The membranes were blocked in 5% milk or 5% BSA in TBST (TBS–Tween 20 (0.1%)) for 1 h at room temperature. Proteins were immunoblotted with the indicated primary antibodies in TBS–Tween 20 (0.1%) containing 1% or 5% BSA for overnight, at +4 °C. Following primary antibodies were used: anti-catalase, 1:1000 (CST, 12980S); anti-RRBP1, 1:1000 (Proteintech, 22015-1-AP); anti-PEX3 antibody, 1:1000 (Schmidt et al., 2012); anti-Pex5, 1:1000 (Invitrogen, PA5-58717); anti-calnexin, 1:1000 (Abcam, 22595); anti-PMP70, 1:800 (Sigma, SAB4200181); anti-GFP, 1:1000 (Aves, GFP-1020); anti-TOM20, 1:500 (CST, 42406); anti-ACOX1, 1:1000 (Proteintech, 10957-1-AP); Anti-ACAA1, 1:2000 (Sigma-MERCK, HPA007244); anti-acetylated tubulin, 1:1000 (Sigma-MERCK, T7451); anti-GAPDH, 1:10000 (Sigma-MERCK, G9545); anti-ATG5, 1:2500 (Proteintech, 10181-2-AP); anti-LC3B 1:1000 (Novus biologicals, 600-1384); anti-VAPB, 1:5000 (Proteintech, 14477-1-AP). Next, the membranes were washed with TBST quickly three times and then three times for 15 min at room temperature on shaker. Then the membranes were incubated with HRP conjugated secondary antibodies against mouse 1:5000 (CST 7076S), rabbit (CST 7074S) or chicken (Promega G135A) in TBST containing 1% BSA for 1 hour at room

temperature on shaker. Then the membranes were washed with TBST quickly three times and then three times for 15 min at room temperature on shocker. ECL western blotting substrate (Thermo Scientific, 32106) was applied to the membrane and chemiluminescence was captured by Chemidoc imaging system (Bio-Rad). Quantification of the bands was performed by Image Lab Software (Bio-Rad).

Immunofluorescence

HEK293T were cultured on 13-mm coverslips 24 h before fixation. Then the media was removed, and the cells were washed three times with PBS. The cells were fixed with 4% paraformaldehyde for 10 min at room temperature and washed three times with PBS. Then the cells were permeabilized with 0.2% Triton X-100 in PBS for 15 min at room temperature and washed with PBS. Next DAPI (1:1000 in PBS) was added for 10 min at room temperature. The cells were washed with PBST (0.1% Tween 20 in PBS) and blocked with 5% BSA in PBST for 2 h at room temperature. The cells were then incubated with corresponding primary antibodies diluted in 5% BSA in PBST overnight at +4 □C. Following primary antibodies were used: anti-catalase, 1:400 (CST, 12980S); anti-RRBP1, 1:500 (GeneTex GT5610); anti-calnexin, 1:1000 (Abcam, 22595); anti-PMP70, 1:150 (Sigma, SAB4200181); anti-GFP, 1:10000 (Aves, GFP-1020); anti-TOM20, 1:250 (CST, 42406); anti-ATPIF, 1:100 (CST 8528). Then the cells were washed with PBST three times for 15 min. The cells were incubated with secondary antibodies diluted 1:1000 in 5% BSA in PBST (anti-mouse Alexa Fluor 555, CST 4409S; anti-mouse Alexa Fluor 647, Invitrogen, A-21235; anti-rabbit Alexa Fluor 555, CST, 4413S; anti-rabbit Alexa Fluor 647, CST, 4414S; anti-chicken Alexa Fluor 488, Invitrogen, A-11039) for 1 h at room temperature and washed with PBST three times for 5 min. Finally, the cells were mounted using antifade mounting media (Vector Laboratories, H-1700-10). The slides were left to dry overnight at room temperature, and then

stored at +4 □C until analysis. The cells were imaged using upright SP8 confocal microscope (Leica).

Quantitative analysis of immunofluorescent images

Imaris Software was used for the analysis of confocal immunofluorescent images. For colocalization analysis Coloc tool within the Surpass system (version 9.5.1) was used. The images were carefully adjusted manually to distinguish between background and signal. The Mander's overlap coefficient was used to quantify the percentage of overlap. In each sample, 5-8 fields of view were analyzed, with each field capturing around 60-120 cells.

To quantify PEX14- or catalase-positive dots, counting cell number or volume, the confocal microscopy images were processed and reconstructed in 3D model using Imaris software. PEX14- or catalase-positive dots were counted using "Dots" function. PEX14 or catalase signal was adjusted for the optimal dot detection: X4 diameter (0.5) and model PSF (1.5). The number of PEX14- catalase-positive dots was normalized to the number of the cells in the specific field of view.

The cell number was counted based on DAPI nuclear staining. Parameters were set with an XY diameter of 7 to optimize nucleus detection. To analyze the cell volume, PEX14 or catalase signal was adjusted to cover the cytosolic area and eliminate any redundant covered regions and debris. Within the Surpass system, a surface was added with default settings, excluding the shortest distance calculations.

Pexophagy assay

RRBP1 KO HEK293T cells expressing EGFP-FLAG-APEX2-ePTS1 or parental cell line were plated on 6-well plate 24 h before the treatment. 100 µM chloroquine was added to the cells

cultured in complete DMEM media. The cells were incubated for 3 h, after the incubation the cells were collected and used for western blotting analysis.

Transmission electron microscopy

RRBP1 KO HEK293T cells expressing EGFP-FLAG-APEX2-ePTS1 or parental cell line were grown on glass coverslips (thickness #1) and fixed with 2% glutaraldehyde (EM-grade) in 0.1 M sodium cacodylate buffer, pH 7.4, supplemented with 2 mM $CaCl_2$. After fixation for 30 min, at RT, the samples were washed with sodium cacodylate buffer followed by washing with 50 mM glysine-sodium hydroxide buffer, pH 10.5. For identification of peroxisomes, the cells expressing APEX2 were labelled with 5 mM 3,3'-diaminobenzidine (DAB) and 0.15% H_2O_2 in glycine-sodium hydroxide buffer for 20 -25 min, on ice, in dark. The reaction was stopped by washing the samples with glycine-sodium hydroxide buffer which after the cells were postfixed with 1% reduced osmium tetroxide in 0.1 M sodium cacodylate buffer for 1 h, on ice. After washing the samples were gradually dehydrated in ethanol and acetone prior flat embedding (Jokitalo et al., 2001) in epoxy (TAAB 812, Aldermaston, UK). Sections of 60 nm were cut using an Ultracut UC7 ultramicrotome (Leica, Vienna, Austria), post-stained with uranyl acetate and lead citrate, and examined at 100 kV using an HT7800 transmission electron microscope (Hitachi High-Technologies, Tokyo, Japan). Images were acquired using a Rio9 CMOS-camera (AMETEK Gatan Inc., Pleasanton, CA).

PO-ER contact site analysis

Three independent experiments were performed. In each experiment for each cell line 13-18 cells having peroxisomal profiles were selected using systematic random sampling for the analysis of peroxisomes and peroxisome-ER contact sites. All the peroxisomes in the selected cells (n = 437 for the parental cell line, n = 403 for the RRBP1 KO cell line) were imaged at 8 000 x nominal

magnification with a pixel size of 1.4 nm. Images were contrast normalized and converted to 8-bit using Microscopy Image Browser (MIB, (Belevich et al., 2016)). For unbiased analysis, the images were anonymized before manually segmenting peroxisomes and ER using MIB. The contact sites were analyzed using the MCcalc plug-in (Lak et al., 2021) in MIB software with probing distance of 150 nm, smoothing 15 and accepting gaps of 7 pixels. The peroxisomal area (peroxisomal size) and eccentricity (peroxisomal shape) were analyzed by MIB software (Belevich et al., 2016).

Statistical Analysis

All data are presented as mean ± standard deviation (SD). For the statistical analyses with two samples, student's unpaired two-tailed t-tests was performed using Graph Pad Prism Software. All the graphs and heat maps were prepared with Graph Pad Prism Software.

ACKNOWLEDGEMENTS

We gratefully acknowledge grant support provided to Cory Dunn from ERC Starting Grant (grant nr. 637649), Academy of Finland, Finland (grant nr. 331556), Jane ja Aatos Erkon Säätiö, Finland (grant nr. 200057) and Sigrid Jusèlius Foundation, Finland. We thank Finnish Cultural Foundation for providing grant to Kaneez Fatima. The HiLife Flow Cytometry Unit at the University of Helsinki and Tiina Pessa-Morikawa are acknowledged for FACS service. Proteomics Unit at the Institute of Biotechnology, University of Helsinki is acknowledged for mass spectrometry analysis of proteins. The Light Microscopy Unit of the Institute of Biotechnology at the University of Helsinki and Marko Crivaro are acknowledged for providing confocal microscopy service. Taina Suntio in the Electron Microscopy Unit (supported by HiLIFE and Biocenter Finland) at the Institute of Biotechnology, University of Helsinki is acknowledged for EM sample preparation.

Maria Vartiainen and Ville Hietakangas are acknowledged for valuable discussion and suggestions. We thank Emilia Kuuluvainen for commenting on the manuscript.

AUTHOR CONTRIBUTIONS

KF designed and performed experiments, analyzed data, wrote the manuscript. HV and EJ performed EM studies. BAA and TS performed experiments. PK discussed the project and commented on the manuscript. SK conceptualized and supervised the project, designed and performed experiments, analyzed data, wrote the manuscript. All authors commented on the manuscript.

CONFLICT OF INTEREST STATEMENT

The authors declare that they have no conflict of interest.

REFERENCES

Akşit, A., and I.J. van der Klei. 2018. Yeast peroxisomes: How are they formed and how do they grow? *Int J Biochem Cell Biol*. 105:24–34. doi:10.1016/J.BIOCEL.2018.09.019.

Albertini, M., P. Rehling, R. Erdmann, W. Girzalsky, J.A.K.W. Kiel, M. Veenhuis, and W.H. Kunau. 1997. Pex14p, a peroxisomal membrane protein binding both receptors of the two PTS-dependent import pathways. *Cell*. 89:83–92. doi:10.1016/S0092-8674(00)80185-3.

Anastasia, I., N. Ilacqua, A. Raimondi, P. Lemieux, R. Ghandehari-Alavijeh, G. Faure, S.L. Mekhedov, K.J. Williams, F. Caicci, G. Valle, M. Giacomello, A.D. Quiroga, R. Lehner, M.J. Miksis, K. Toth, T.Q. de Aguiar Vallim, E. V. Koonin, L. Scorrano, and L. Pellegrini. 2021. Mitochondria-rough-ER contacts in the liver regulate systemic lipid homeostasis. *Cell Rep*. 34. doi:10.1016/J.CELREP.2021.108873/ATTACHMENT/C935BB5D-0203-4599-9051-7D9ADFF4B483/MMC7.XLSX.

Balboa, D., J. Weltner, S. Eurola, R. Trokovic, K. Wartiovaara, and T. Otonkoski. 2015. Conditionally Stabilized dCas9 Activator for Controlling Gene Expression in Human Cell Reprogramming and Differentiation. *Stem Cell Reports*. 5:448–459. doi:10.1016/J.STEMCR.2015.08.001.

Baldwin, H.A., C. Wang, G. Kanfer, H. V. Shah, A. Velayos-Baeza, M. Dulovic-Mahlow, N. Brüggemann, A. Anding, E. Baehrecke, D. Maric, W.A. Prinz, and R.J. Youle. 2021. VPS13D promotes peroxisome biogenesis. *J Cell Biol*. 220. doi:10.1083/JCB.202001188.

Belevich, I., M. Joensuu, D. Kumar, H. Vihinen, and E. Jokitalo. 2016. Microscopy Image Browser: A Platform for Segmentation and Analysis of Multidimensional Datasets. *PLoS Biol*. 14:e1002340. doi:10.1371/JOURNAL.PBIO.1002340.

Cardoen, B., K.R. Vandevoorde, G. Gao, M. Ortiz-Silva, P. Alan, W. Liu, E. Tiliakou, A.W. Vogl, G. Hamarneh, and I.R. Nabi. 2024. Membrane contact site detection (MCS-DETECT) reveals dual control of rough mitochondria-ER contacts. *J Cell Biol*. 223. doi:10.1083/JCB.202206109/VIDEO-9.

Costello, J.L., I.G. Castro, C. Hacker, T.A. Schrader, J. Metz, D. Zeuschner, A.S. Azadi, L.F. Godinho, V. Costina, P. Findeisen, A. Manner, M. Islinger, and M. Schrader. 2017. ACBD5 and VAPB mediate membrane associations between peroxisomes and the ER. *Journal of Cell Biology*. 216:331–342. doi:10.1083/JCB.201607055/VIDEO-2.

Demers, N.D., V. Riccio, D.S. Jo, S. Bhandari, K.B. Law, W. Liao, C. Kim, G.A. McQuibban, S.K. Choe, D.H. Cho, and P.K. Kim. 2023. PEX13 prevents pexophagy by regulating ubiquitinated PEX5 and peroxisomal ROS. *Autophagy*. 19:1781–1802. doi:10.1080/15548627.2022.2160566.

Diefenbach, R.J., E. Diefenbach, M.W. Douglas, and A.L. Cunningham. 2004. The ribosome receptor, p180, interacts with kinesin heavy chain, KIF5B. *Biochem Biophys Res Commun*. 319:987–992. doi:10.1016/j.bbrc.2004.05.069.

Dimitrov, L., S.K. Lam, and R. Schekman. 2013. The Role of the Endoplasmic Reticulum in Peroxisome Biogenesis. *Cold Spring Harb Perspect Biol*. 5. doi:10.1101/CSHPERSPECT.A013243.

Distel, B., R. Erdmann, S.J. Gould, G. Blobel, D.I. Crane, J.M. Cregg, G. Dodt, Y. Fujiki, J.M. Goodman, W.W. Just, J.A.K.W. Kiel, W.H. Kunau, P.B. Lazarow, G.P. Mannaerts, H.W. Moser, T. Osumi, R.A. Rachubinski, A. Roscher, S. Subramani, H.F. Tabak, T. Tsukamoto, D. Valle, I. Van Der Klei, P.P. Van Veldhoven, and M. Veenhuis. 1996. A unified nomenclature for peroxisome biogenesis factors. *Journal of Cell Biology*. 135:1–3. doi:10.1083/JCB.135.1.1.

Erdmann, R., M. Veenhuis, D. Mertens, and W.H. Kunau. 1989. Isolation of peroxisome-deficient mutants of Saccharomyces cerevisiae. *Proceedings of the National Academy of Sciences*. 86:5419–5423. doi:10.1073/PNAS.86.14.5419.

Fang, Y., J.C. Morrell, J.M. Jones, and S.J. Gould. 2004. PEX3 functions as a PEX19 docking factor in the import of class I peroxisomal membrane proteins. *Journal of Cell Biology*. 164:863–875. doi:10.1083/JCB.200311131.

Fujiki, Y., K. Okumoto, S. Mukai, M. Honsho, and S. Tamura. 2014. Peroxisome biogenesis in mammalian cells. *Front Physiol*. 5 AUG:102311. doi:10.3389/FPHYS.2014.00307/BIBTEX.

Germain, K., and P.K. Kim. 2020. Pexophagy: A Model for Selective Autophagy. *Int J Mol Sci*. 21. doi:10.3390/IJMS21020578.

Geuze, H.J., J.L. Murk, A.K. Stroobants, J.M. Griffith, M.J. Kleijmeer, A.J. Koster, A.J. Verkleij, B. Distel, and H.F. Tabak. 2003. Involvement of the endoplasmic reticulum in peroxisome formation. *Mol Biol Cell*. 14:2900–2907. doi:10.1091/MBC.E02-11-0734.

Goldman, B.M., and G. Blobel. 1978. Biogenesis of peroxisomes: intracellular site of synthesis of catalase and uricase. *Proc Natl Acad Sci U S A*. 75:5066–5070. doi:10.1073/PNAS.75.10.5066.

Guillén-Samander, A., M. Leonzino, M.G. Hanna, N. Tang, H. Shen, and P. De Camilli. 2021. VPS13D bridges the ER to mitochondria and peroxisomes via Miro. *J Cell Biol*. 220. doi:10.1083/JCB.202010004.

Hasan, S., H.W. Platta, and R. Erdmann. 2013. Import of proteins into the peroxisomal matrix. *Front Physiol*. 4. doi:10.3389/FPHYS.2013.00261.

Hua, R., D. Cheng, É. Coyaud, S. Freeman, E. Di Pietro, Y. Wang, A. Vissa, C.M. Yip, G.D. Fairn, N. Braverman, J.H. Brumell, W.S. Trimble, B. Raught, and P.K. Kim. 2017. VAPs and ACBD5 tether peroxisomes to the ER for peroxisome maintenance and lipid homeostasis. *Journal of Cell Biology*. 216:367–377. doi:10.1083/JCB.201608128.

Hung, V., S.S. Lam, N.D. Udeshi, T. Svinkina, G. Guzman, V.K. Mootha, S.A. Carr, and A.Y. Ting. 2017. Proteomic mapping of cytosol-facing outer mitochondrial and ER membranes in living human cells by proximity biotinylation. *Elife*. 6. doi:10.7554/ELIFE.24463.

Hung, V., N.D. Udeshi, S.S. Lam, K.H. Loh, K.J. Cox, K. Pedram, S.A. Carr, and A.Y. Ting. 2016. Spatially resolved proteomic mapping in living cells with the engineered peroxidase APEX2. *Nature Protocols 2016 11:3*. 11:456–475. doi:10.1038/nprot.2016.018.

Jokitalo, E., N. Cabrera-Poch, G. Warren, and D.T. Shima. 2001. Golgi clusters and vesicles mediate mitotic inheritance independently of the endoplasmic reticulum. *J Cell Biol*. 154:317. doi:10.1083/JCB.200104073.

Killackey, S.A., Y. Bi, D.J. Philpott, D. Arnoult, and S.E. Girardin. 2023. Mitochondria-ER cooperation: NLRX1 detects mitochondrial protein import stress and promotes mitophagy through the ER protein RRBP1. *Autophagy*. 19:1601. doi:10.1080/15548627.2022.2129763.

Klouwer, F.C.C., K.D. Falkenberg, R. Ofman, J. Koster, D. van Gent, S. Ferdinandusse, R.J.A. Wanders, and H.R. Waterham. 2021. Autophagy Inhibitors Do Not Restore Peroxisomal Functions in Cells With the Most Common Peroxisome Biogenesis Defect. *Front Cell Dev Biol*. 9:661298. doi:10.3389/FCELL.2021.661298/BIBTEX.

Konovalova, S., X. Liu, P. Manjunath, S. Baral, N. Neupane, T. Hilander, Y. Yang, D. Balboa, M. Terzioglu, L. Euro, M. Varjosalo, and H. Tyynismaa. 2018. Redox regulation of GRPEL2 nucleotide exchange factor for mitochondrial HSP70 chaperone. *Redox Biol*. 19:37. doi:10.1016/J.REDOX.2018.07.024.

Konovalova, S., R. Torregrosa-Muñumer, P. Manjunath, X. Liu, S. Baral, K. Fatima, M. Holopainen, J. Kvist, J. Rajendran, Y. Yang, M. Varjosalo, R. Käkelä, P. Somerharju, and H. Tyynismaa. 2023. Small mitochondrial protein NERCLIN regulates cardiolipin homeostasis and mitochondrial ultrastructure. *Proc Natl Acad Sci U S A*. 120. doi:10.1073/PNAS.2210599120/-/DCSUPPLEMENTAL.

Koppers, M., N. Özkan, H.H. Nguyen, D. Jurriens, J. McCaughey, R. Stucchi, M. Altelaar, L.C. Kapitein, C.C. Hoogenraad, and G.G. Farias. 2022. Axonal ER tubules regulate local translation via P180/RRBP1-mediated ribosome interactions. *bioRxiv*. 2022.11.30.518484. doi:10.1101/2022.11.30.518484.

Kors, S., C. Hacker, C. Bolton, R. Maier, L. Reimann, E.J.A. Kitchener, B. Warscheid, J.L. Costello, and M. Schrader. 2022. Regulating peroxisome–ER contacts via the ACBD5-VAPB tether by FFAT motif phosphorylation and GSK3β. *Journal of Cell Biology*. 221. doi:10.1083/JCB.202003143/212956.

Kurochkin, I. V., Y. Mizuno, A. Konagaya, Y. Sakaki, C. Schönbach, and Y. Okazaki. 2007. Novel peroxisomal protease Tysnd1 processes PTS1- and PTS2-containing enzymes involved in β-oxidation of fatty acids. *EMBO J*. 26:835. doi:10.1038/SJ.EMBOJ.7601525.

Lak, B., S. Li, I. Belevich, S. Sree, R. Butkovic, E. Ikonen, and E. Jokitalo. 2021. Specific subdomain localization of ER resident proteins and membrane contact sites resolved by electron microscopy. *Eur J Cell Biol*. 100:151180. doi:10.1016/J.EJCB.2021.151180.

Lam, S.K., N. Yoda, and R. Schekman. 2010. A vesicle carrier that mediates peroxisome protein traffic from the endoplasmic reticulum. doi:10.1073/pnas.1013397107.

Lam, S.S., J.D. Martell, K.J. Kamer, T.J. Deerinck, M.H. Ellisman, V.K. Mootha, and A.Y. Ting. 2014. Directed evolution of APEX2 for electron microscopy and proximity labeling. *Nature Methods 2014 12:1*. 12:51–54. doi:10.1038/nmeth.3179.

Lam, S.S., J.D. Martell, K.J. Kamer, T.J. Deerinck, M.H. Ellisman, V.K. Mootha, and A.Y. Ting. 2015. Directed evolution of APEX2 for electron microscopy and proximity labeling. *Nat Methods*. 12:51–54. doi:10.1038/NMETH.3179.

Liu, X., K. Salokas, F. Tamene, Y. Jiu, R.G. Weldatsadik, T. Öhman, and M. Varjosalo. 2018. An AP-MS- and BioID-compatible MAC-tag enables comprehensive mapping of protein interactions and subcellular localizations. *Nat Commun*. 9. doi:10.1038/S41467-018-03523-2.

Martell, J.D., T.J. Deerinck, S.S. Lam, M.H. Ellisman, and A.Y. Ting. 2017. Electron microscopy using the genetically encoded APEX2 tag in cultured mammalian cells. *Nat Protoc*. 12:1792. doi:10.1038/NPROT.2017.065.

Matsumoto, N., S. Tamura, and Y. Fujiki. 2003. The pathogenic peroxin Pex26p recruits the Pex1p-Pex6p AAA ATPase complexes to peroxisomes. *Nat Cell Biol*. 5:454–460. doi:10.1038/NCB982.

Miura, S., M. Mori, M. Takiguchi, M. Tatibana, S. Furuta, S. Miyazawa, and T. Hashimoto. 1984. THE JOURNAL OF BIOLOGICAL CHEMISTRY Biosynthesis and Intracellular Transport of Enzymes of Peroxisomal @-Oxidation*. 259. doi:10.1016/S0021-9258(20)82155-3.

Ogawa-Goto, K., K. Tanaka, T. Ueno, K. Tanaka, T. Kurata, T. Sata, and S. Irie. 2007. p180 Is Involved in the Interaction between the Endoplasmic Reticulum and Microtubules through a Novel Microtubule-binding and Bundling Domain. *Mol Biol Cell*. 18:3741. doi:10.1091/MBC.E06-12-1125.

Okumoto, K., N. Miyata, and Y. Fujiki. 2018. Identification of peroxisomal protein complexes with PTS receptors, pex5 and pex7, in mammalian cells. *Subcell Biochem*. 89:287–298. doi:10.1007/978-981-13-2233-4_12/FIGURES/4.

Rachubinski, R.A., Y. Fujiki, R.M. Mortensen, and P.B. Lazarow. 1984. Acyl-Coa oxidase and hydratase-dehydrogenase, two enzymes of the peroxisomal beta-oxidation system, are synthesized on free polysomes of clofibrate-treated rat liver. *Journal of Cell Biology*. 99:2241–2246. doi:10.1083/JCB.99.6.2241.

Rae, J., C. Ferguson, N. Ariotti, R.I. Webb, H.H. Cheng, J.L. Mead, J.D. Riches, D.J.B. Hunter, N. Martel, J. Baltos, A. Christopoulos, N.S. Bryce, M.L. Cagigas, S. Fonseka, M.E. Sayre, E.C. Hardeman, P.W. Gunning, Y. Gambin, T.E. Hall, and R.G. Parton. 2021. A robust method for particulate detection of a genetic tag for 3D electron microscopy. *Elife*. 10. doi:10.7554/ELIFE.64630.

Ran, F.A., P.D. Hsu, J. Wright, V. Agarwala, D.A. Scott, and F. Zhang. 2013. Genome engineering using the CRISPR-Cas9 system. *Nat Protoc*. 8:2281. doi:10.1038/NPROT.2013.143.

Rubinson, D.A., C.P. Dillon, A. V. Kwiatkowski, C. Sievers, L. Yang, J. Kopinja, M. Zhang, M.T. McManus, F.B. Gertler, M.L. Scott, and L. Van Parijs. 2003. A lentivirus-based system to functionally silence genes in primary mammalian cells, stem cells and transgenic mice by RNA interference. *Nat Genet*. 33:401–406. doi:10.1038/NG1117.

Sakai, Y., M. Oku, I.J. van der Klei, and J.A.K.W. Kiel. 2006. Pexophagy: Autophagic degradation of peroxisomes. *Biochimica et Biophysica Acta (BBA) - Molecular Cell Research*. 1763:1767–1775. doi:10.1016/J.BBAMCR.2006.08.023.

Savitz, A.J., and D.I. Meyer. 1990. Identification of a ribosome receptor in the rough endoplasmic reticulum. *Nature 1990 346:6284*. 346:540–544. doi:10.1038/346540a0.

Schliebs, W., J. Saidowsky, B. Agianian, G. Dodt, F.W. Herberg, and W.-H. Kunau. 1999. Recombinant Human Peroxisomal Targeting Signal Receptor PEX5. *Journal of Biological Chemistry*. 274:5666–5673. doi:10.1074/jbc.274.9.5666.

Schmid-Burgk, J.L., K. Höning, T.S. Ebert, and V. Hornung. 2016. CRISPaint allows modular base-specific gene tagging using a ligase-4-dependent mechanism. *Nat Commun*. 7. doi:10.1038/NCOMMS12338.

Schmidt, F., D. Dietrich, R. Eylenstein, Y. Groemping, T. Stehle, and G. Dodt. 2012. The role of conserved PEX3 regions in PEX19-binding and peroxisome biogenesis. *Traffic*. 13:1244–1260. doi:10.1111/J.1600-0854.2012.01380.X.

Sengupta, R., M.J. Poderycki, and S. Mattoo. 2019. CryoAPEX - an electron tomography tool for subcellular localization of membrane proteins. *J Cell Sci*. 132. doi:10.1242/JCS.222315/VIDEO-2.

Shibata, Y., T. Shemesh, W.A. Prinz, A.F. Palazzo, M.M. Kozlov, and T.A. Rapoport. 2010. Mechanisms determining the morphology of the peripheral ER. *Cell*. 143:774. doi:10.1016/J.CELL.2010.11.007.

Somborac, T., G. Lutfullahoglu Bal, K. Fatima, H. Vihinen, A. Paatero, E. Jokitalo, V.O. Paavilainen, and S. Konovalova. 2023. The subset of peroxisomal tail-anchored proteins do not reach peroxisomes via ER, instead mitochondria can be involved. *PLoS One*. 18:e0295047. doi:10.1371/JOURNAL.PONE.0295047.

Titorenko, V.I., and R.A. Rachubinski. 2008. Chapter 5 Spatiotemporal Dynamics of the ER□derived Peroxisomal Endomembrane System. *Int Rev Cell Mol Biol*. 272:191–244. doi:10.1016/S1937-6448(08)01605-5.

Walter, T., and R. Erdmann. 2019. Current Advances in Protein Import into Peroxisomes. *Protein J*. 38:351–362. doi:10.1007/S10930-019-09835-6.

Van Der Zand, A., I. Braakman, and H.F. Tabak. 2010. Peroxisomal Membrane Proteins Insert into the Endoplasmic Reticulum. *Mol Biol Cell*. 21:2057. doi:10.1091/MBC.E10-02-0082.

FIGURE LEGENDS

Figure 1. Systematic identification of peroxisomal biogenesis factors using proximity labeling.

(A) Overview of the APEX2-based proximity labeling approach to identify peroxisomal biogenesis factors. (B) Western blotting analysis of HEK293T clonal cell lines stably expressing GFP-APEX2-ePTS1 or GFP-APEX2 constructs. GAPDH or tubulin was used as a loading control. (C) Live-cell fluorescent microscopy images showing intracellular localization of GFP-APEX2-ePTS1 or GFP-APEX2 constructs in HEK293T cells. The localization of GFP-containing constructs was visualized using green channel. Scale bar, 20 μm. (D) Filtering steps of mass spectrometry data to identify highly confident peroxisomal biogenesis factors candidates (E) Heat map of peroxisomal biogenesis factors after filtering.

Figure 2. CRISPR/Cas9 microscopy-based screen of the potential peroxisomal biogenesis factors identified by proximity labeling.

(A) Overview of the CRISPR/Cas9 microscopy-based screen. (B) Heat map of CRISPR/Cas9 microscopy assessing the phenotype of HEK293T cells. HEK293T cells stably expressing GFP-APEX2-ePTS1 were transiently transfected with gRNAs and Cas9-mCherry plasmid as shown in (A). Two rounds of transfection were performed (I and II). Each round the phenotype of the cells was assessed three times at 7, 10 and 14 post-transfection days using live-cell fluorescent microscopy. The phenotype of the cells was scored based on the localization of GFP signal from 0 to 3, where 0 corresponds to GFP localized in puncta and 3 is for strong mislocalization of GFP to cytosol. gRNAs targeting PEX5 or PEX19 were used as positive controls. The top three candidates are in red. (C) Live-cell fluorescent microscopy images of HEK293T cells stably expressing GFP-APEX2-ePTS1 before and after 13 days of transfection with Cas9-mCherry plasmid and gRNA

targeting RRBP1, PEX5 or PEX19. The localization of peroxisomal targeted construct GFP-APEX2-ePTS1 was visualized using green channel. Scale bar, 50 μm.

Figure 3. RRBP1 is required for peroxisomal maintenance in human cells.

(A) Western blot analysis of RRBP1 KO HEK293T cells stably expressing GFP-APEX2-ePTS1. Parental, PEX3 and PEX19 KO HEK293 cells without peroxisomal targeted construct were used as controls. GAPDH was used as a loading control. (B) Quantification of peroxisomal protein levels using western blot images represented in (A) (n = 3-4). (C) Quantification of ACOX1 processing using western blot images represented in (A) (n = 3-4). (D) Quantification of ER protein levels using western blot images represented in (A) (n = 3-5). (E) Quantification of TOM20 protein level using western blot images represented in (A) (n = 3-4). In all graphs data are presented as mean ± SD. *P < 0.05, **P < 0.01, ***P < 0.001, ****P < 0.0001, ns, not significant as compared to the parental cell line (unpaired t-tests).

Figure 4. The number of peroxisomes is decreased in RRBP1 KO cells.

(A) Live-cell fluorescent microscopy images showing intracellular localization of stability expressing GFP-APEX2-ePTS1 construct in RRBP1 KO or parental HEK293T cells. The localization of GFP-containing constructs was visualized using green channel. Scale bar, 10 μm. (B) Confocal microscopy analysis of RRBP1 KO or parental HEK293T cells stably expressing GFP-APEX2-ePTS1. Immunostaining was performed using anti-PEX14, anti-GFP, anti-catalase or anti-RRBP1 antibody. Scale bar, 5 μm. (C) The number of PEX14- or catalase-positive dots was analyzed in RRBP1 KO or parental HEK293T cells stably expressing GFP-APEX2-ePTS1. Z-

stacks of confocal microscopy images were processed and reconstructed in 3D model with Imaris software. Each value represents analysis of around 100 cells. (D) The volume of RRBP1 KO or parental HEK293T cells stably expressing GFP-APEX2-ePTS1 was analyzed using confocal microscopy images. Z-stacks of confocal microscopy images were processed and reconstructed in 3D model with Imaris software. Each value represents analysis of around 100 cells. PEX14 or Catalase signal was used for the analysis. In all graphs data are presented as mean ± SD. *P < 0.05, **P < 0.01, ***P < 0.001, ****P < 0.0001, ns, not significant as compared to the parental cell line (unpaired t-tests).

Figure 5. RRBP1 silencing causes peroxisomal deficiency in human cells.

(A) Western blot analysis of RRBP1 silencing in HEK293T cells stably expressing GFP-APEX2-ePTS1. The cells were transfected with corresponding esiRNAs for 72 h. GFP esiRNA was used as a negative control, esiRNA PEX5 was used as a positive control. (B-D) Quantification of western blot images presented in (A) (n = 3 in (B) and (D), n = 4 in (C). GAPDH or tubulin was used as a loading controls. In all graphs data are presented as mean ± SD. *P < 0.05, **P < 0.01, ns, not significant (unpaired t-tests). (E) Live-cell fluorescent microscopy images of cells HEK293T cells stably expressing GFP-APEX2-ePTS1 before and after transfection with indicated esiRNAs. The localization of peroxisomal targeted construct GFP-APEX2-ePTS1 was visualized using green channel. GFP esiRNA was used as a negative control, esiRNA PEX5 was used as a positive control. Scale bar, 25 μm.

Figure 6. The decreased number of peroxisomes in RRBP1 KO cells is independent of pexophagy.

(A) Western blot analysis of RRBP1 KO or parental HEK293T cells stability expressing GFP-APEX2-ePTS1 construct before and after treatment with 100 μM chloroquine for 3 h. GAPDH was used as a loading control. (B) Quantification of western blot images presented in (A) (n = 3). In all graphs data are presented as mean ± SD. *P < 0.05, **P < 0.01, ns, not significant (unpaired t-tests).

Figure 7. RRBP1 does not localize to peroxisomes.

(A) Intracellular localization of RRBP1 was analyzed in HEK293T cells using immunofluorescent confocal microscopy. Catalase was used to label peroxisomes, ATPIF1was used to visualize mitochondria, calnexin was used to label ER. Scale bar, 3 μm. (B) Colocalization analysis of confocal microscopy images represented in (A) by Mander's overlap coefficient. The data are presented as mean ± SD.

Figure 8. RRBP1 KO affects peroxisome-ER contact sites.

(A) Confocal microscopy imaging of RRBP1 KO or parental HEK293T cells stably expressing GFP-APEX2-ePTS1. Anti-calnexin antibody was used to label ER, anti-PMP70 was used to visualize peroxisomes, anti-TOM20 antibody was used to label mitochondria. Arrows indicate peroxisomes found in closed proximity to ER. Scale bar, 3 μm. (B) Colocalization analysis of confocal microscopy images represented in (A) by Mander's overlap coefficient. (C) Representative electron microscopy images of RRBP1 KO or parental HEK293T cells stably expressing GFP-APEX2-ePTS1. Peroxisomes were labeled by DAB staining. Scale bar, 200 nm. PO, peroxisome; ER, endoplasmic reticulum. (D) Relative distribution of peroxisome-ER contact sites at two distances in RRBP1 KO or parental HEK293T cells stability expressing GFP-APEX2-ePTS1

construct analyzed by electron microscopy images. In each experiment for each cell line 13-18 cells having peroxisomal profiles were selected using systematic random sampling. All the peroxisomes in the selected cells were imaged (n = 105 - 175 for each replicate of parental cell line, n = 84 - 168 for each replicate of RRBP1 KO cell line) and the peroxisomal-ER distances were analyzed using Microscopy Image Browser (MIB, (Belevich et al., 2016)). (E) The distribution of the peroxisomal area (peroxisomal size) analyzed in RRBP1 KO (n = 437) or parental HEK293T cells (n = 403) stably expressing GFP-APEX2-ePTS1. Electron microscopy images and Microscopy Image Browser (MIB, (Belevich et al., 2016)) were used for the analysis. (F) Eccentricity (peroxisomal shape) was analyzed using electron microscopy images and Microscopy Image Browser (MIB, (Belevich et al., 2016)). In all graphs data are presented as mean ± SD. *P < 0.05, ***P < 0.001, ns, not significant as compared to the parental cell line (unpaired t-tests).

Fig. 1: Systematic identification of peroxisomal biogenesis factors using proximity labeling

A

Construct	HEK293T	Biotinylation targets
None	Parental	Background
GFP-APEX2-ePTS1	Parental	Peroxisomal proteins
	PEX3 KO	Peroxisomal biogenesis factors
	PEX19 KO	
GFP-APEX2	Parental	Background
	PEX3 KO	
	PEX19 KO	

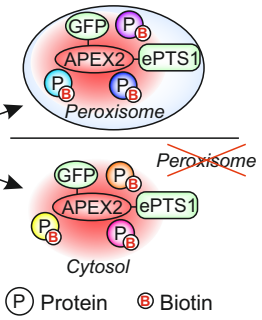

D

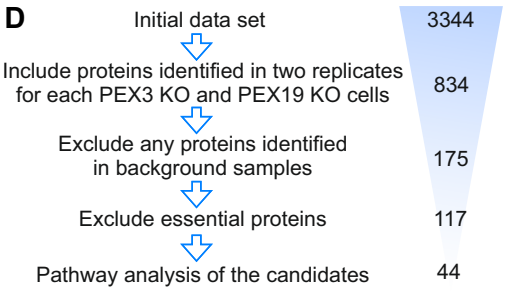

B

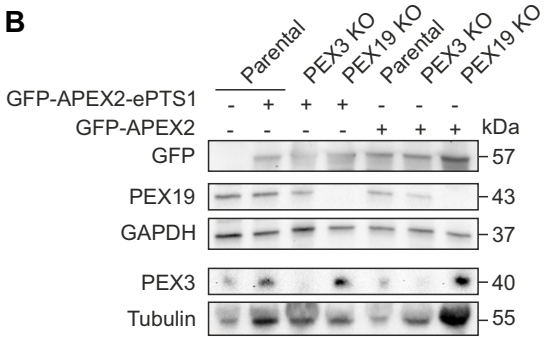

C

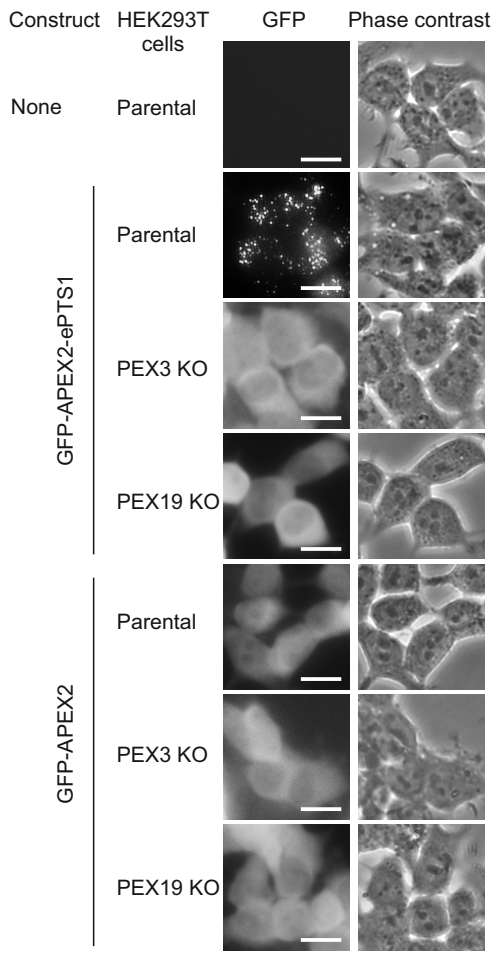

E

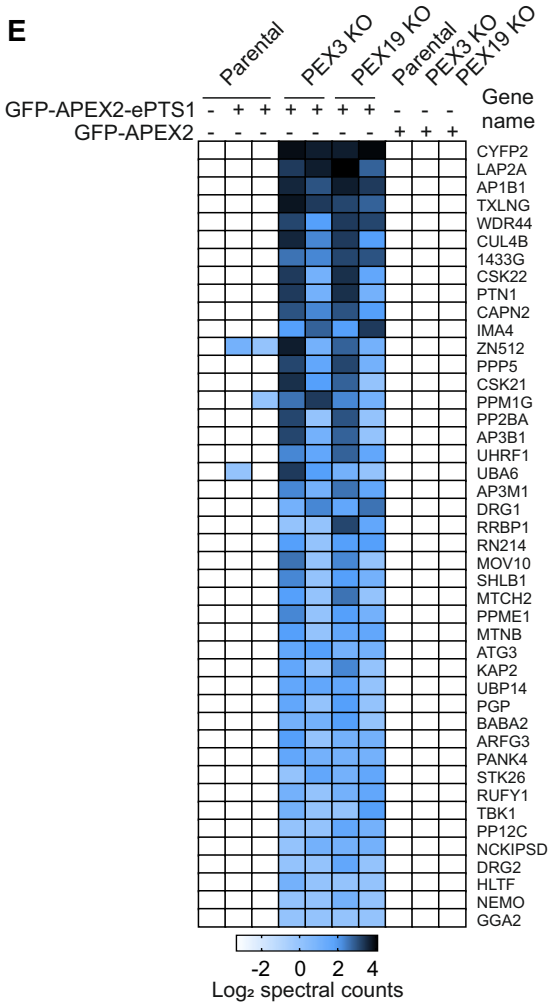

Fig. 2: CRISPR/Cas9 microscopy-based screen of the potential peroxisomal biogenesis factors identified by proximity labeling

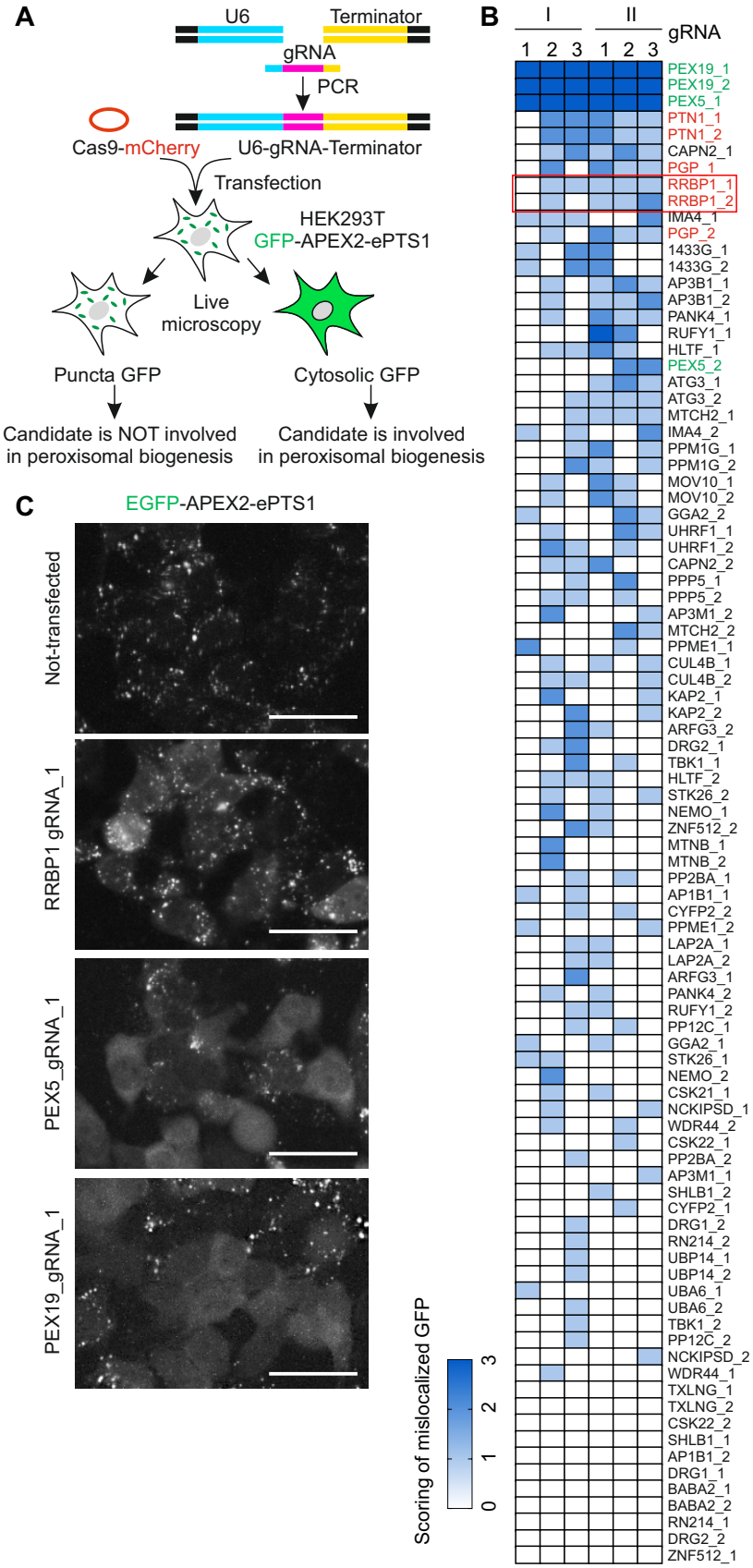

Fig. 3: RRBP1 is required for peroxisomal maintenance in human cells

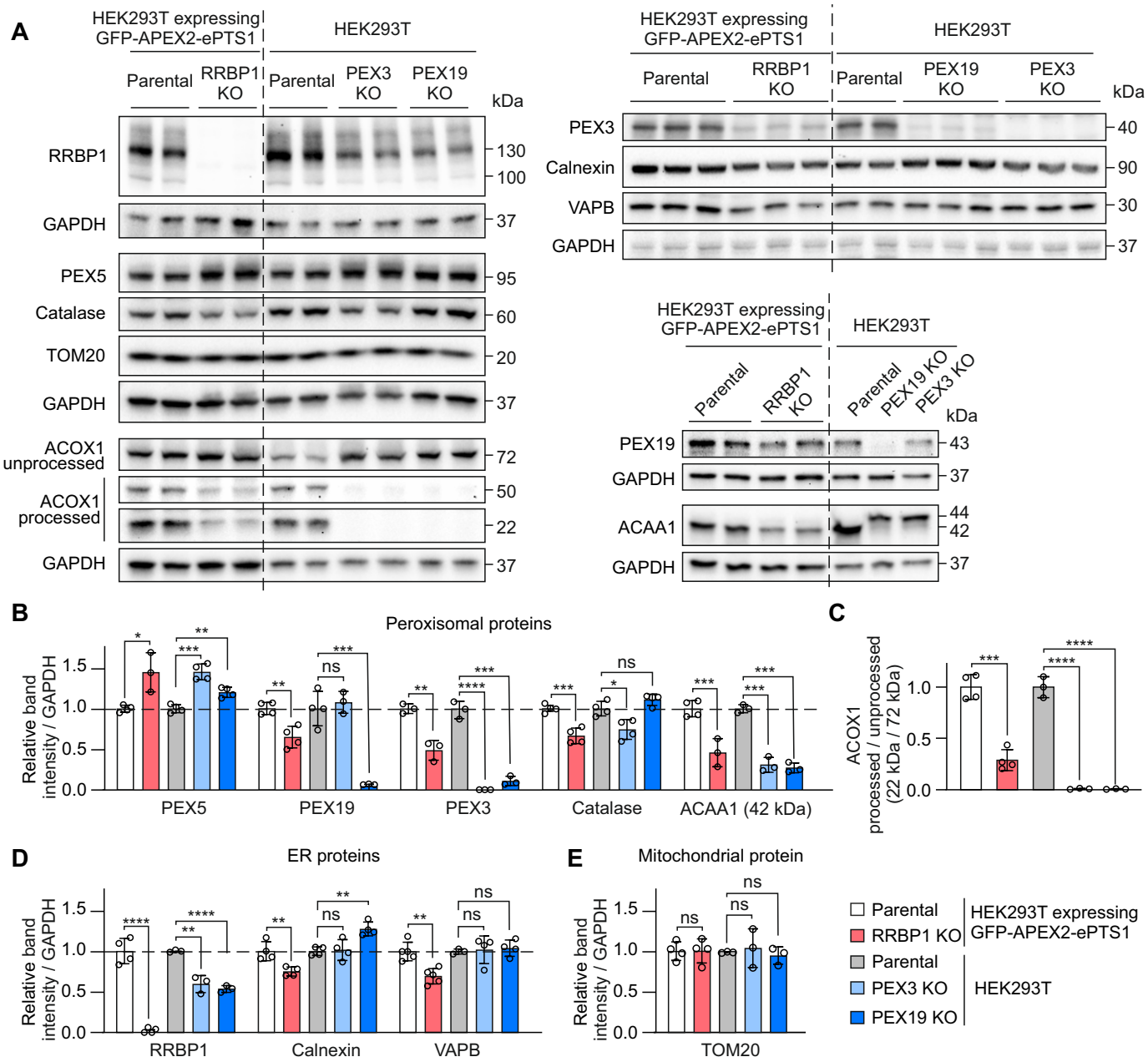

Fig. 4: The number of peroxisomes is decreased in RRBP1 KO cells

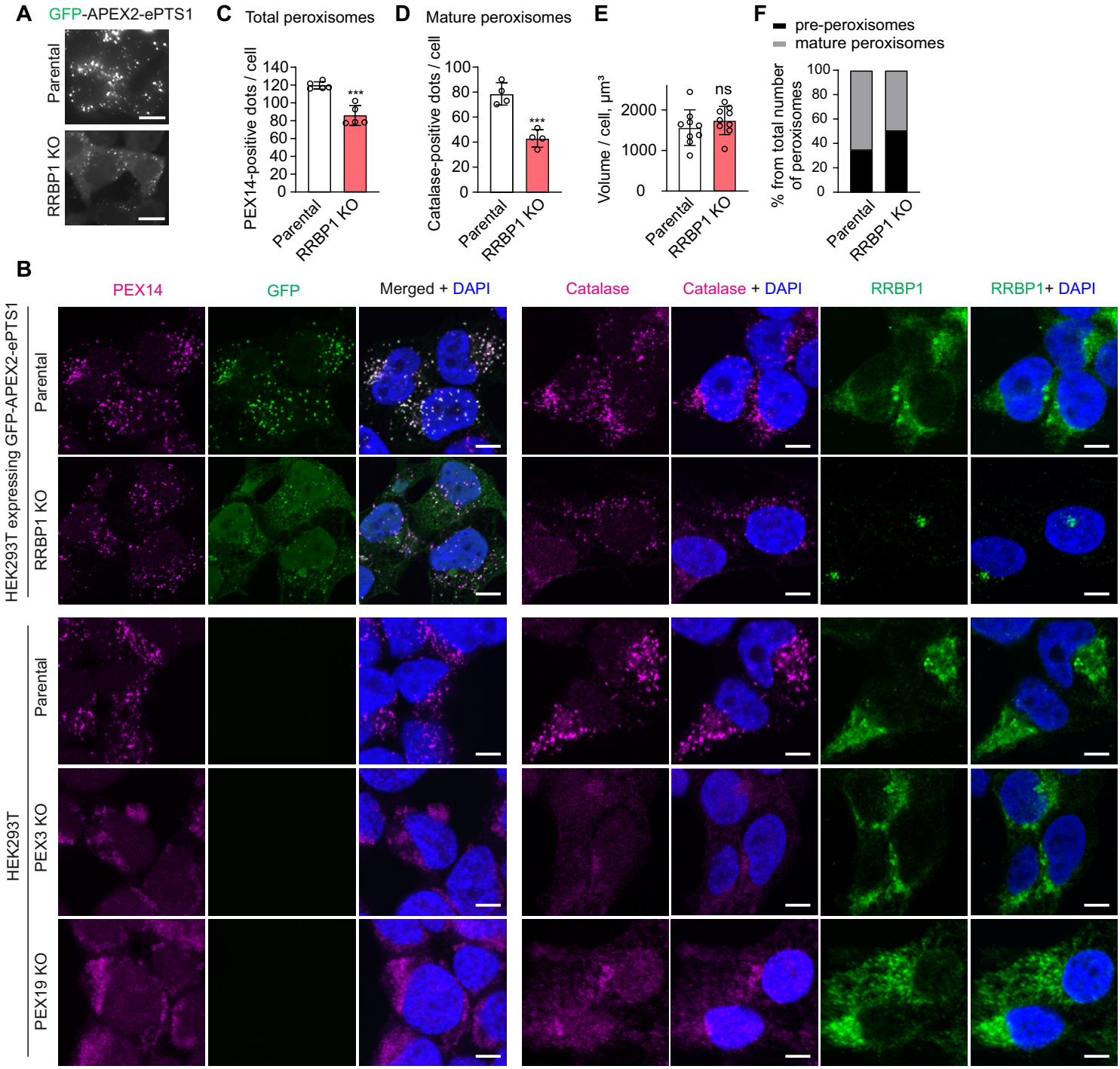

Fig. 5: RRBP1 silencing causes peroxisomal deficiency in human cells

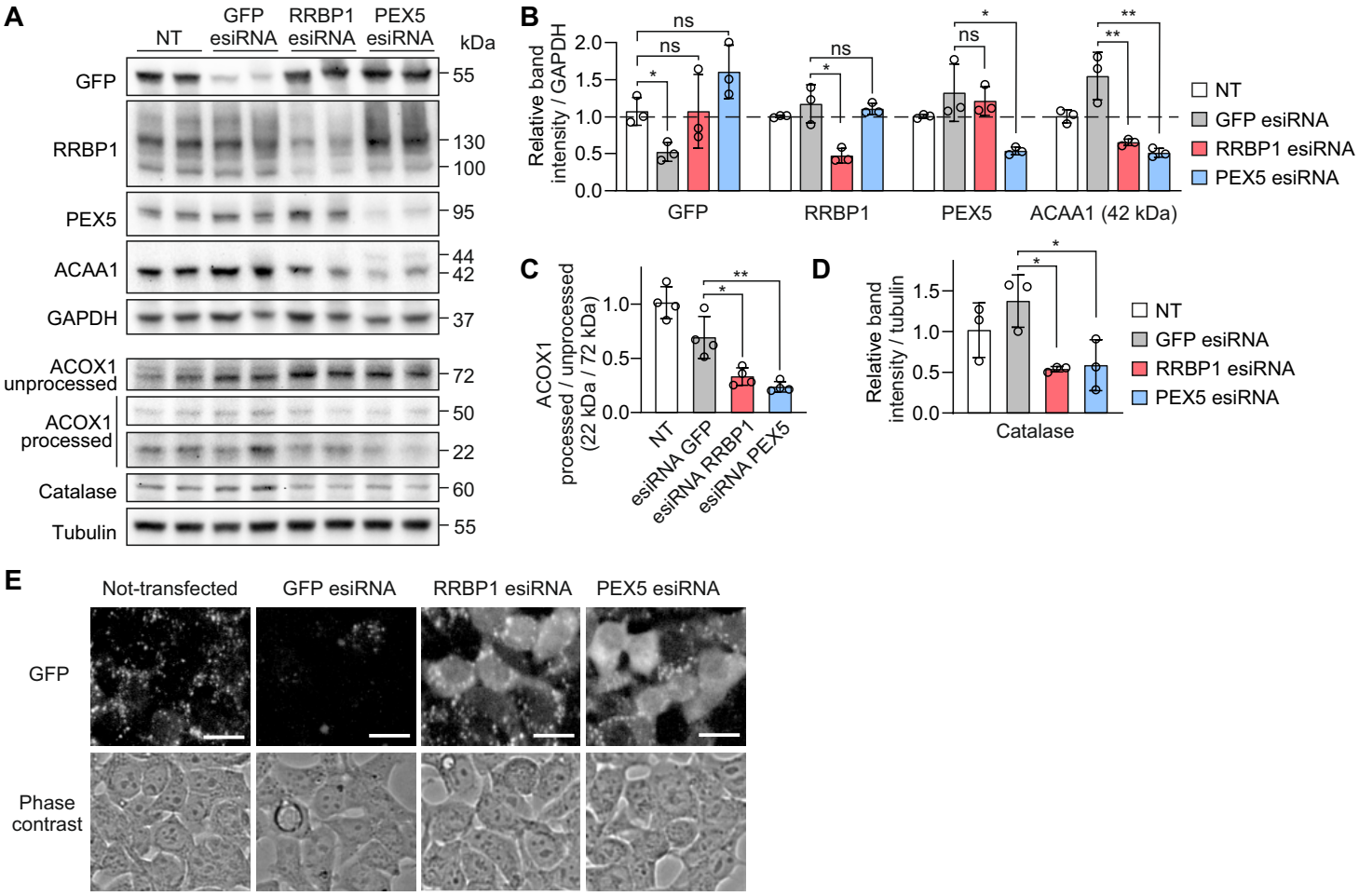

Fig. 6: The loss of peroxisomes in RRBP1 KO cells is independent of pexophagy

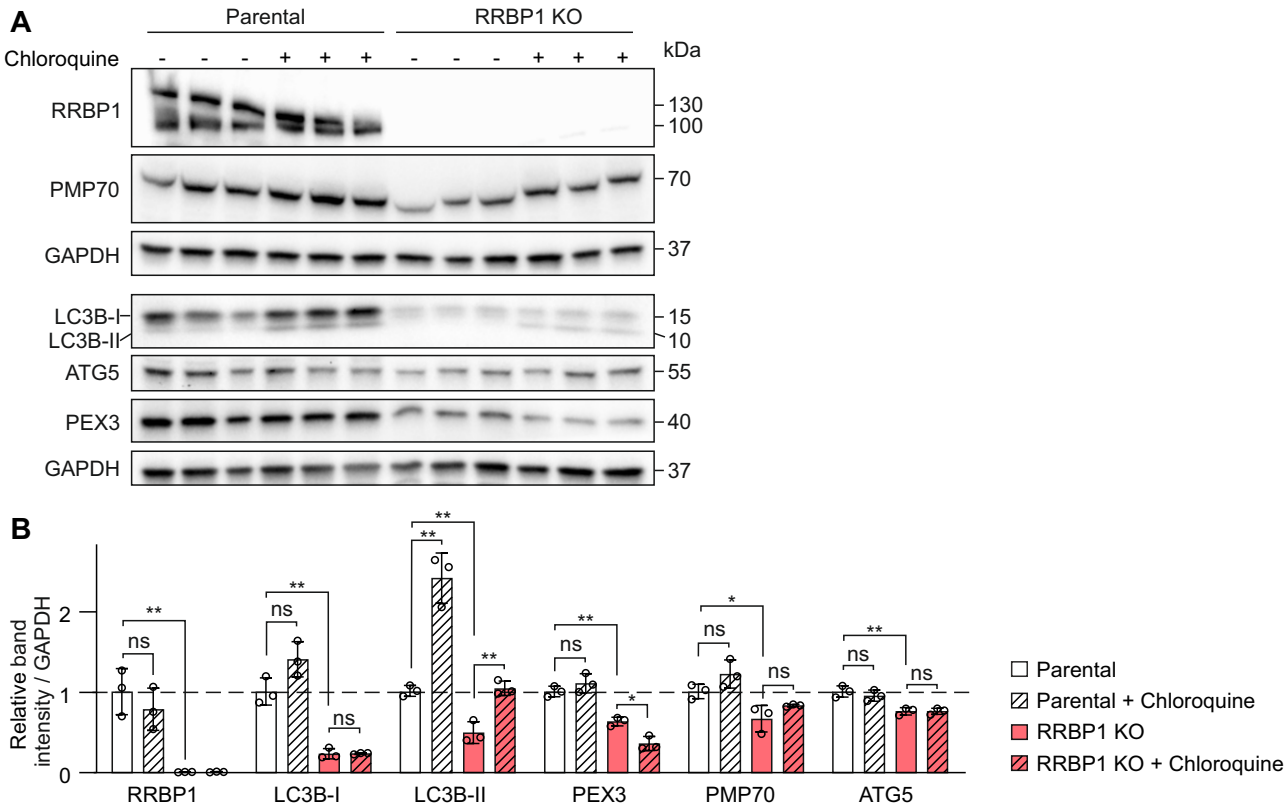

Fig. 7: RRBP1 does not localize to peroxisomes

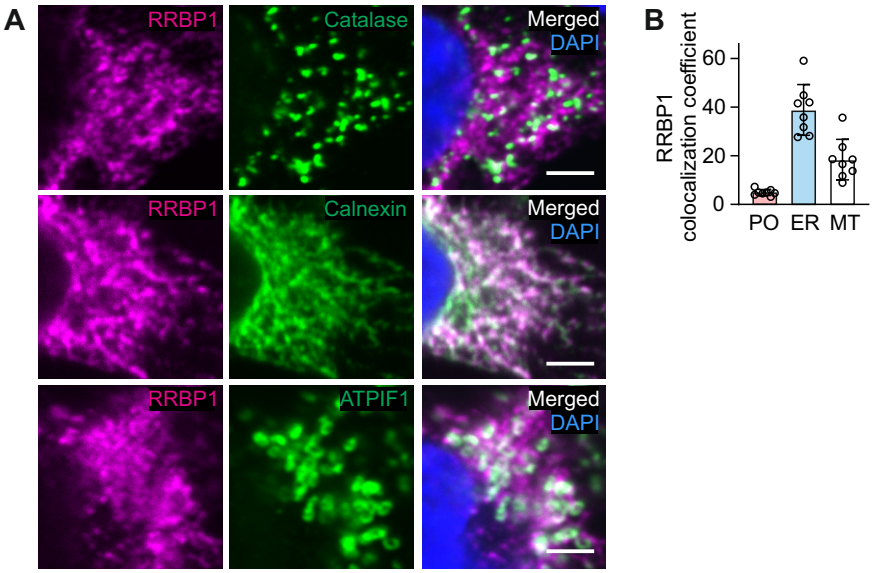
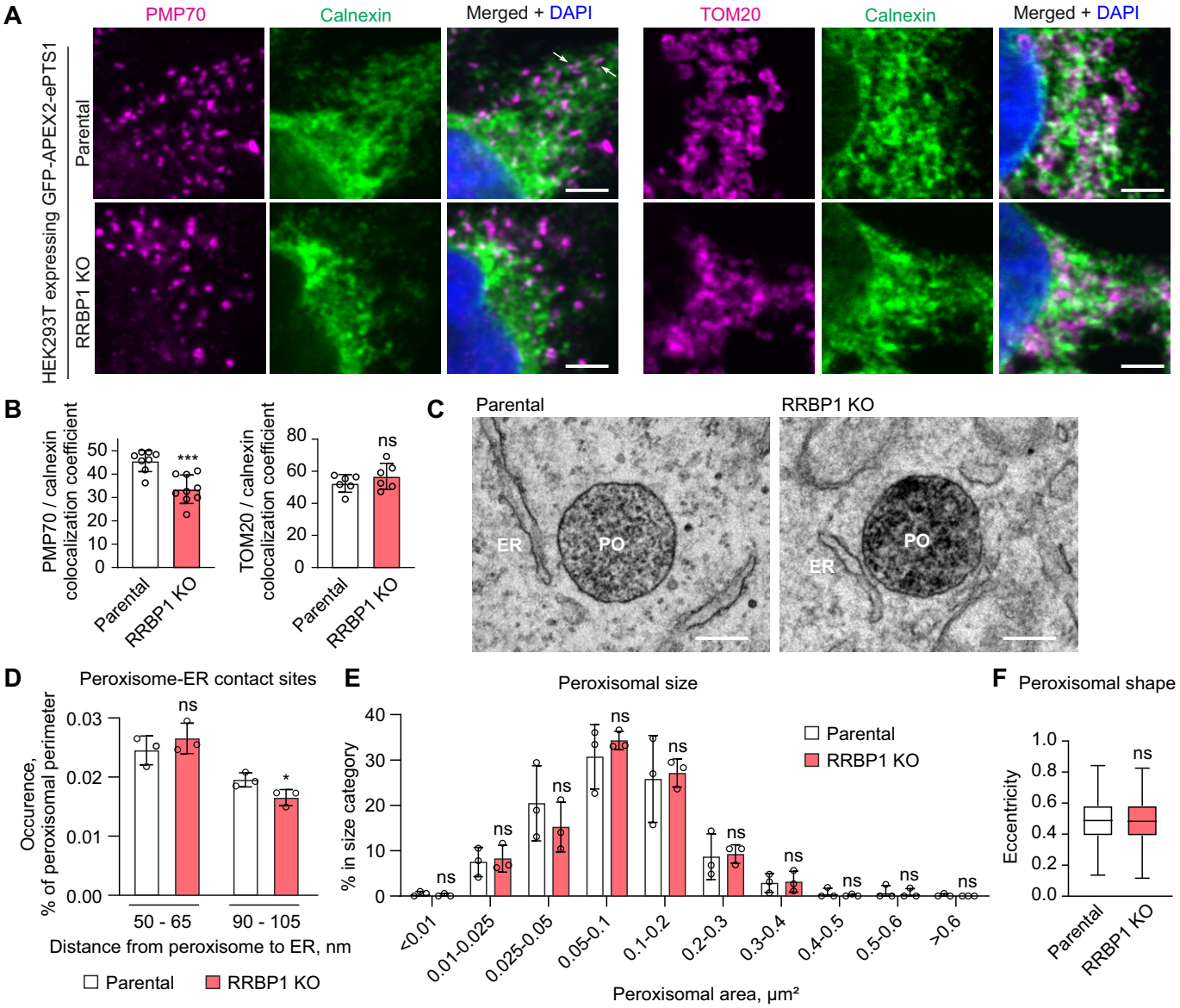
Fig. 8: RRBP1 KO affects peroxisome-ER contact sites